Applied Catalysis B: Environmental 200 (2017) 343–350

Contents lists available at ScienceDirect

Applied Catalysis B: Environmental

journal homepage: www.elsevier.com/locate/apcatb

Macroscopically shaped monolith of nanodiamonds @ nitrogen-enriched mesoporous carbon decorated SiC as a superior metal-free catalyst for the styrene production

Housseinou Ba[a,1], Jingjie Luo[a,c,1], Yuefeng Liu[a,b,*], Cuong Duong-Viet[a], Giulia Tuci[d], Giuliano Giambastiani[d,e], Jean-Mario Nhut[a], Lam Nguyen-Dinh[f], Ovidiu Ersen[c], Dang Sheng Su[b], Cuong Pham-Huu[a,*]

[a] Institut de Chimie et Procédés pour l'Energie, l'Environnement et la Santé (ICPEES), ECPM, UMR 7515 du CNRS- University of Strasbourg (UdS), 25 rue Becquerel, 67087 Strasbourg, Cedex 02, France
[b] Dalian National Laboratory for Clean Energy (DNL), Dalian Institute of Chemical Physics, Chinese Academy of Sciences, 457 Zhongshan Road, 116023 Dalian, China
[c] Institut de Physique et Chimie des Matériaux de Strasbourg (IPCMS), UMR 7504, CNRS-University of Strasbourg (UdS), 23, rue du Loess, 67034 Strasbourg, Cedex 02, France
[d] Institute of Chemistry of OrganoMetallic Compounds, ICCOM-CNR and Consorzio INSTM, Via Madonna del Piano, 10-50019, Sesto F.no, Florence, Italy
[e] Kazan Federal University, 420008 Kazan, Russian Federation
[f] The University of Da-Nang, University of Science and Technology, 54 Nguyen Luong Bang, Da-Nang, Viet Nam

ARTICLE INFO

Article history:
Received 17 March 2016
Received in revised form 29 June 2016
Accepted 14 July 2016
Available online 15 July 2016

Keywords:
Metal-free catalysis
Macroscopically shaped monoliths
Nanodiamonds
Food-grade components
Direct dehydrogenation of ethylbenzene

ABSTRACT

Nanodiamonds (NDs) are recognized as a class of robust metal-free catalysts for the steam-free, direct dehydrogenation (DDH) of ethylbenzene (EB) to styrene (ST). In spite of that, some main drawbacks, such as their powdery form along with their tendency to form aggregates, limit their full exploitation at the industrial level. In this work, we describe the preparation of macroscopically shaped monoliths consisting of silicon carbide-based foams coated with a nitrogen-rich mesoporous carbon matrix (NMC) as a non-innocent glue for highly dispersed ND fillers. The NMC phase is prepared from cheap and non-toxic food-grade components and it prevents the undesired NDs agglomeration thus maximizing the reagents exposure throughout the catalytic DDH tests. Moreover, the NMC phase represents a key source of surface basicity capable of inhibiting the occurrence of EB cracking side reactions during the catalytic runs. As a result, the ND@NMC/SiC composite shows excellent dehydrogenation performance already at low ND loading if compared with the powdery NDs and/or the SiC-supported NDs of the state-of-the-art. Noteworthy, the ND@NMC/SiC composite presents its best catalytic performance under DDH conditions close to those used in industrial plants (reaction temperture up to 600 °C and EB concentrations up to 10 vol.%) with high ST rates ($\lambda_{catal.}$ of 9.9 $mmol_{ST}\ g_{cat}^{-1}\ h^{-1}$), ST selectivity over 96% and long term stability on stream.

1. Introduction

Styrene (ST) is mainly produced by the gas-phase direct dehydrogenation (DDH) of ethylbenzene (EB) [1–3]. The most widely employed catalyst for such reaction is a low surface area iron-based oxide promoted with different elements such as alumina or potassium [4,5]. Nowadays, about 85% of the ST worldwide production is realized by means of these catalysts, which typically operate under high temperatures (ranging from 580 to 630 °C). The iron-based catalysts are cheap and they can ensure relatively high ST selectivity in the process. However, these metal-based catalysts list a number of serious disadvantages that significantly limit their catalytic performance, e.g. the drastic deactivation/passivation of their metal active sites due to the rapid generation of "coke" deposits. To overcome this problem, a large amount of steam is generally co-feeded in the reactor with heavy energy wastes, estimated to be around 1.5×10^9 cal per ton of ST produced, together with large amounts of waste water containing traces of hydrocarbons which need to be purified before being discharged. Moreover,

* Corresponding authors at: Institut de Chimie et Procédés pour l'Energie, l'Environnement et la Santé (ICPEES), ECPM, UMR 7515 du CNRS- University of Strasbourg (UdS), 25 rue Becquerel, Cedex 02, Strasbourg 67087, France.
E-mail addresses: yuefeng.liu@dicp.ac.cn, yuefeng.liu@unistra.fr (Y. Liu), cuong.pham-huu@unistra.fr (C. Pham-Huu).
[1] These authors contributed equally.

http://dx.doi.org/10.1016/j.apcatb.2016.07.014
0926-3373/

the use of steam is responsible of other serious limitations and namely: (i) the side consumption of reagent (EB) and product (ST) by steam-reforming, (ii) the chemical reaction of steam with the Fe promoter (i.e. K_2CO_3) leading to the gradual and irreversible catalyst deactivation. Thus, the search for less energy-demanding catalytic materials with high activity and stability as well as coke-resistance, low active phase leaching, high structural resistance and low or nil steam demand represents a challenging issue towards the development of sustainable DDH processes and catalysts. On this ground, carbon nanomaterials, including carbon nanotubes/nanofibers and graphene, preferentially doped with nitrogen atoms, have been widely investigated in the last decade as efficient metal-free catalysts for a number of key catalytic transformations, i.e. the electrochemical oxygen reduction reaction (ORR) [6–8], the selective oxidation of impurities for gas cleaning[9–12] and the alkane dehydrogenations[13–15] just to mention a few.

In the recent years, the sp^3-hybridized nanodiamonds (NDs) have also gained great interest by the material science and catalysis community[16–28] due to their unique physico-chemical properties such as a large surface to volume ratio [29], a high thermal conductivity as well as easy ways to functionalize their outer surface [19,20,30,31]. Among the most representative applications of NDs in catalysis, Su and co-workers have demonstrated how these systems behave as excellent metal-free candidates for the steam-free, direct dehydrogenation of EB with activities (λ expressed as $mmol_{ST}\ g_{ND}^{-1}\ h^{-1}$) at the steady-state conditions up to 2.8 times higher than those measured with the benchmark commercial K-promoted iron catalyst (K-Fe) and remarkably high ST selectivity [1]. Furthermore, NDs are extremely stable systems under the operative steam-free DDH conditions and their active surface is preserved from the formation of coke deposits even after long reaction times. Since this seminal contribution, the development of carbon-based nanomaterials, including light-hetero doped carbons, as metal-free catalysts for the steam-free DDH of EB [32–35] has received a rapid boost. Recent issues have demonstrated how the N-doping of the ND surface [31] or its coating by a layer of carbon nitride [34], can generate "modified NDs" with improved catalytic performance in the EB DDH. Indeed, N-doping gives rise to an electronic modification of the neighboring carbon atoms thus improving the material adsorption properties as well as their inherent catalytic performance in the process [27,36–42]. Moreover, the basic surface character of the modified systems is expected to have beneficial effects on the ultimate catalyst performance by suppressing or reducing the occurrence of EB cracking side-reactions [14,15,34,43–48].

One main challenging issue in heterogeneous catalysis deals with the control of the morphological properties of a solid catalyst. Indeed, its final performance in catalysis is controlled by the effective active sites exposure as well as by the control of the reagent(s)/product(s) accessibility and diffusion throughout the material. NDs are classically produced by detonation method [16,17], and they show a high tendency to form agglomerates. This tendency reduces the exposure of their effective surface thus limiting their exploitation as catalysts. On this regard, the idea of improving the dispersion of NDs thus increasing the effective surface available per weight sounds as a challenging matter of great priority finalized at improving their catalytic performance. On this ground, hybrid materials consisting of ND particles uniformly dispersed on graphene oxide and/or few-layer-graphene (FLG) sheets, have significantly improved the DDH activity, showing λ values of 1.7 and 3.4 times higher, respectively, once compared with the bulk NDs under identical experimental conditions [32,49]. In spite of that, NDs supported on 2D carbons are still in the form of powders and this can lead to significant pressure drops along the catalyst bed including serious limitations linked to the catalyst handling and transportation [50]. Liu et al. [33] have recently proposed a two-step synthetic approach for the anchoring of NDs aggregates on carbon nanotubes (CNTs) decorated SiC macroscopic supports. The as prepared and easy-to-handle ND/CNT-SiC monoliths have successfully been used as metal-free catalysts in the steam-free DDH of EB. In a recent work from some of us [50], a facile one-step synthesis has been proposed to the production of new hybrid structures consisting of NDs decorated β-SiC foams. These macroscopic ND/β-SiC composites, featured by an uniform dispersion of NDs at the surface of the porous SiC network, display remarkably low pressure drops together with DDH activities several times higher compared to those of bulk NDs and the industrial K-promoted iron catalyst under identical steam-free conditions. Although the aforementioned methods already constitute a significant step forward in the NDs technology for heterogeneous catalysis applications, there is still a lot of room available and much work to be done for preparing macroscopic and robust monoliths featuring a highly dispersed ND-phase as efficient metal-free catalysts for the steam-free EB dehydrogenation. In addition, high DDH catalytic performance and high stability of carbon-based materials under drastic reaction conditions (high temperatures and high EB concentrations in the feed) still represent ambitious tasks to be faced. From an industrial point of view, the development of macroscopically shaped hybrid systems featured by highly dispersed NDs, preferably in a N-rich carbon-based matrix, along with improved mechanical stability, can answer the need of safe materials (in terms of handling, use and transportation) with excellent catalytic performance in the DDH process.

Herein, we describe the preparation of highly dispersed NDs (as fillers) into an N-rich mesoporous carbon coating (NMC) for macroscopically shaped β-SiC supports. The commercial NDs with a diameter ranging from 5 to 10 nm are dispersed and sonicated in an aqueous solution of non-toxic, food-grade components (i.e. ammonium carbonate, D-glucose and citric acid) [14,51] and the as-prepared suspension is used as impregnating bath for the β-SiC support to be soaked. Successive thermal treatments of the impregnated β-SiC generate N-doped, mesoporous carbonaceous surface coatings containing highly dispersed ND fillers (ND@NMC). Besides playing a key role of catalytic sites for the DDH process (*vide infra*) NDs hold the additional role of nucleation centers for the growth of the mesoporous NMC-phase. This latter is localized around the NDs and it largely prevents the fillers agglomeration without limiting diffusion of the reagent (EB) and product(s), from and to the ND surface. Noteworthy, the straightforward soaking procedure used for the impregnation of the support with the pre-catalyst active phase, opens the way to the use of various macroscopic scaffolds (SiC in the form of grains, extrudates, foams or beads) to be selected depending on the catalyst downstream application.

β-SiC is widely recognized as an ideal catalyst support for several industrial applications [33,52–60] thanks to its unique chemico-physical properties. Its high mechanical stability along with its good thermal conductivity [61,62] and chemical inertness make it an excellent support for nanocarbons in the endothermic steam-free DDH reaction. A β-SiC foam is then selected as support of choice for the present study and the resulting 3D composite (ND@NMC/SiC) has been systematically investigated in the steam-free DDH of EB into ST under various experimental conditions (temperature and EB concentrations).

2. Experimental section

2.1. Materials preparation

Nanodiamonds (ND) were purchased from the Carbodeon *Ltd* Oy (Finland) and were used without any further treatment. The fabrication of the macroscopic ND@NMC/SiC sample is illustrated

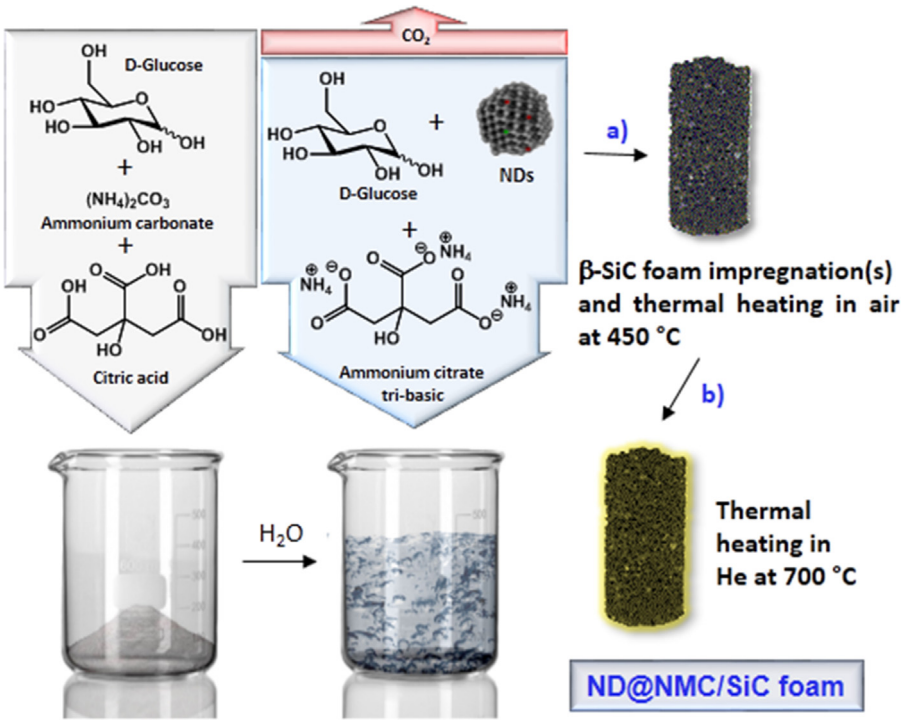

Fig. 1. Schematic representation of the synthetic procedure adopted for the synthesis of the ND@NMC/SiC composite.

in Fig. 1. In a typical procedure, D-Glucose (2 g) and citric acid (3 g) are dissolved in 10 mL of ultrapure Milli-Q water at room temperature (r.t.). A proper amount of ammonium carbonate (3 g) is then added in a single portion to the solution at room temperature and an instantaneous effervescence due to CO_2 evolution is observed. 2 g of ND aggregates are then added in one portion to the solution and the resulting suspension is sonicated at r.t. for 20 min to give a homogeneous NDs dispersion.

To fabricate the macroscopic ND@NMC/SiC composite (Fig. 1), the as-prepared suspension is used to impregnate the supports, i.e. SiC foam (30 $m^2\,g^{-1}$; SICAT). The wet solid has been dried in air at room temperature and it is impregnated again in the same suspension. The wet solid undergoes a gentle heating in air from r.t. to 130 °C (10 °C min^{-1}) and it is kept at this temperature for 5 h. The solid is then submitted to two successive thermal treatments: (a) under air at 450 °C for 2 h (heating rate of 2 °C min^{-1} from r.t. to 450 °C); b) under He at 700 °C for 5 h (heating rate of 10 °C min^{-1} from r.t. to 700 °C). The first heating phase generates the nitrogen-doped mesoporous carbon coating containing the dispersed NDs while the successive thermal heating at 700 °C improves the ND@NMC phase adhesion to the SiC surface. This latter thermal phase with better graphitization degree is also expected to improve the final electrical and thermal conductivity of the SiC surface coating.

The as-prepared composite is designated as follows: ND@NMC/SiC. For the sake of comparison, the same synthetic methodology is applied to the preparation of a ND-free composite (blank sample – NMC/SiC). In this case a homogeneous solution of ammonium carbonate, citric acid and glucose was used as impregnating phase for the SiC support. The nitrogen-free composite (defined as ND@MC/SiC) is also prepared without ammonium carbonate in the mixture solution by using the aforementioned synthetic process. The soaked SiC matrix undergoes identical thermal treatments [51].

2.2. Characterization techniques

The scanning electron microscopy (SEM) is carried out on a JEOL 2600F with a resolution of 5 nm. The sample is deposited onto a double face graphite tape in order to avoid problems of charging effects during the analysis. The TEM analysis is carried out on a JEOL 2100F (available at IPCMS – UMR 7504 of the CNRS) working at 200 kV accelerated voltage, equipped with a probe corrector for spherical aberrations, and a point-to-point resolution of 0.2 nm. The thermal gravimetric analysis (TGA) is performed on a TA Instruments Model Q-5000. The amount of each sample (4–10 mg max) is loaded into a platinum crucible and heated in air from room temperature to 1000 °C with a heating rate of 10 °C min^{-1}. The N_2 adsorption-desorption measurements are run on a Micromeritics® sorptometer. Each analyzed sample is outgassed at 250 °C under ultra-high vacuum for 8 h in order to desorb moisture and all adsorbed volatile species. XPS measurements are run on a MULTILAB 2000 (THERMO VG) spectrometer equipped with Al Kα anode ($h\nu$ = 1486.6 eV) with 10 min of acquisition. Peak deconvolution is realized with the "Avantage" program from Thermoelectron Company. The C 1 s peak at 284.6 eV is used to correct all charging effects. Shirley backgrounds are then subtracted from the raw data to obtain the areas of the C 1 s peak. Temperature-programmed oxidation experiment is performed in a Micromeritics ASAP-2100 setup equipped with a multichannel mass spectrometer. Typical sample (5 mg) is loaded in the reactor and then flushed with 1% O_2/He mixture (25 mL min^{-1}) at room temperature (RT) for 30 min. The oxidation products are monitored with m/e intensity of 44 for CO_2 at the temperature range from RT to 900 °C (10 °C min^{-1}).

2.3. Catalytic dehydrogenation experiments

The steam-free catalytic dehydrogenation of EB to ST is carried out on a fixed-bed continuous flow reactor under atmospheric pressure. The catalyst (300 mg) is loaded onto a quartz fritted disk

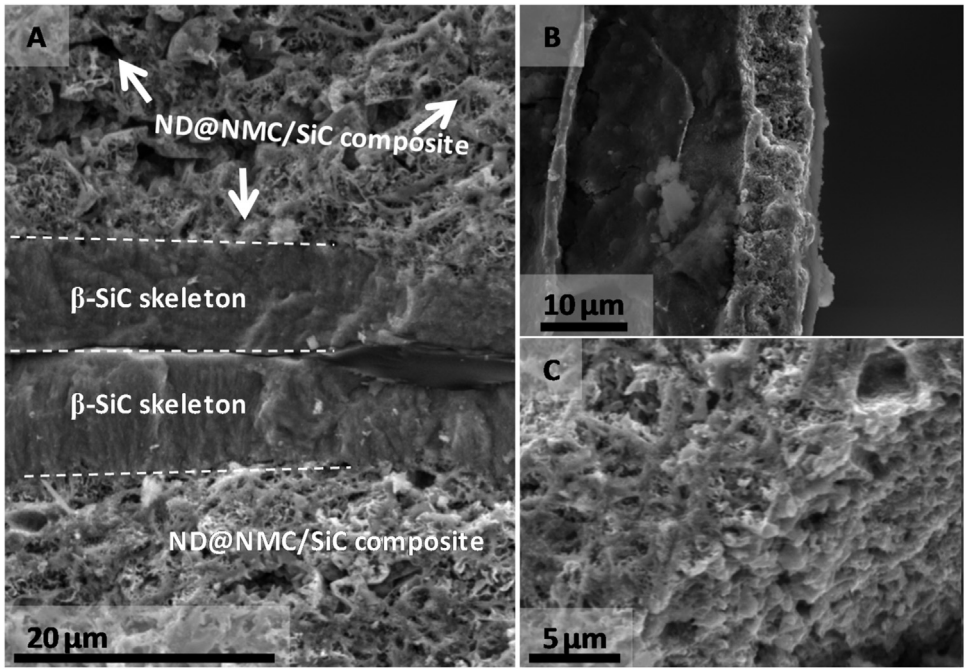

Fig. 2. (A, B) SEM images of the ND@NMC coating on the β-SiC support with different magnifications. (C) High magnification SEM micrograph showing the porous structure of the ND/NMC coating layer.

located inside a tubular quartz reactor (id × l: 8 mm × 800 mm). Helium gas is then fed into the reactor at a flow rate of 30 mL min^{-1} using a mass flow controller (BROOKS MFC) and passed through a glass evaporator filled with liquid EB maintained at 40 °C thanks to an external thermally regulated bath (EB partial pressure of 2922 Pa). The helium flow containing EB is passed downward through the catalytic bed.

The reaction system is heated at the target temperature (550 or 600 °C) and kept for 2 h under He flow. The reactant flow (2.8, 4.7 or 10 vol.% EB diluted in helium, total flow rate of 30 mL min^{-1}) is then fed into the reactor at the selected reaction temperature (550 or 600 °C). Reactant (EB) and products [styrene (ST), benzene (BZ) and toluene (TOL)] are analyzed on-line at the reactor outlet with a PERICHROM (PR 2100) gas chromatography equipped with a flame detector (FID) and a previously calibrated CP WAX S2CB column. In order to avoid any possible condensation of reactant and/or products, all pipe lines are wrapped with a heating wire that keeps the temperature at 110 °C.

EB conversions (X_{EB}), ST selectivity (S_{ST}), ST rates (λ) and ST yields (Y_{ST}) are calculated according to the following Eqs. (1)–(4):

$$X_{EB}[\%] = \left(1 - \frac{FC_{EB,outlet}}{F_0 C_{EB,inlet}}\right) \times 100 \quad (1)$$

$$S_{ST}[\%] = \frac{C_{ST,outlet}}{(C_{ST,outlet} + C_{TOL,outlet} + C_{BZ,outlet})} \times 100 \quad (2)$$

$$Y_{ST}[\%] = X_{EB} \times S_{ST} \quad (3)$$

$$\lambda_{catalyst}[mmol_{ST} g_{catal.} h^{-1}] = \frac{F \times Y_{ST} \times C_{ST,outlet}}{m_{catalyst} \times t} \quad (4)$$

where F and F_0 are the flow rates at the reactor outlet and inlet, respectively, C_{EB}, C_{ST}, C_{TOL} and C_{BZ} represent the concentration of EB, ST, toluene and benzene, respectively. The carbon balance is around 100% for all experiments.

3. Results and discussion

3.1. Chemico-physical and morphological study of the ND@NMC/SiC composite

With the aim at preparing catalytic materials suitable for industrial application, the ND@NMC active phase has been supported on a macroscopically shaped matrix as to have an easy-to-handle catalytic material possibly featured by sufficiently high mass transfer and low pressure drop [50,53]. On this regard, a suspension prepared by dispersing NDs in a homogeneous solution of cheap food-grade components (ammonium carbonate, citric acid and glucose) is used as impregnating phase for a selected β-SiC foam to be soaked (Fig. 1). Afterwards, the impregnated foam undergoes two controlled thermal treatments, at 450 °C under air and 700 °C under inert atmosphere, respectively. The TGA analysis was used to roughly calculate the ND@NMC loading at the SiC support. Unfortunately, this technique failed in the attempt of distinguishing between ND content and NMC phase irrespective to the analysis programs and conditions (air *vs.* N_2) used. The SiC surface coating (ND@NMC) was found to be around 11 wt% (Fig. S1E) that was even lower (in wt%) of the pure NMC phase at the ND-free NMC/SiC blank sample (15 wt%, Fig. S1C) and nitrogen-free ND@MC/SiC sample (14 wt%, Fig. S1D). The TGA profile of the literature ND/SiC composite [50] is also reported for the sake of comparison (Fig. S1B) and its ND loading (13 wt% of NDs) will be matter for discussion in the catalytic performance of the various composites at work (*vide infra*). SEM images are used to investigate the surface morphology at the ND@NMC/SiC composite. As Fig. 2 shows, the ND@NMC coating presents a highly porous texture and it appears homogeneously fixed to the β-SiC support. Additional evidence for the homogeneous and tight ND@NMC coating at the SiC surface is definitively provided by TEM analysis (Fig. S2). The EXD analysis at the ND@NMC coating is finally used to get more details on the material surface composition. Fig. 3 unambiguously shows the uniform distribution of the hetero-elements (namely N, O) at the SiC coating and confirms the high N-concentration at the topmost material surface. The ultrasonic method is finally performed for testing the

Table 1
Physico-chemical characterization of the materials and precursors.

Samples	BET_{SSA} (m^2g^{-1})	D_{BJH} (nm)	V_{total} (cm^3g^{-1})	C at%	O at%	Si at%	N at%
SiC	28	20	0.15	33.6	25.3	41.1	–
ND	258	16	1.27	92.8	7.2	–	–
ND/SiC	73	14	0.26	81.4	13.0	5.7	–
NMC/SiC	57	12.8	0.13	53.6	21.4	16.9	8.1
ND@NMC/SiC	104	6.5	0.13	61.3	15.2	13.5	10.0

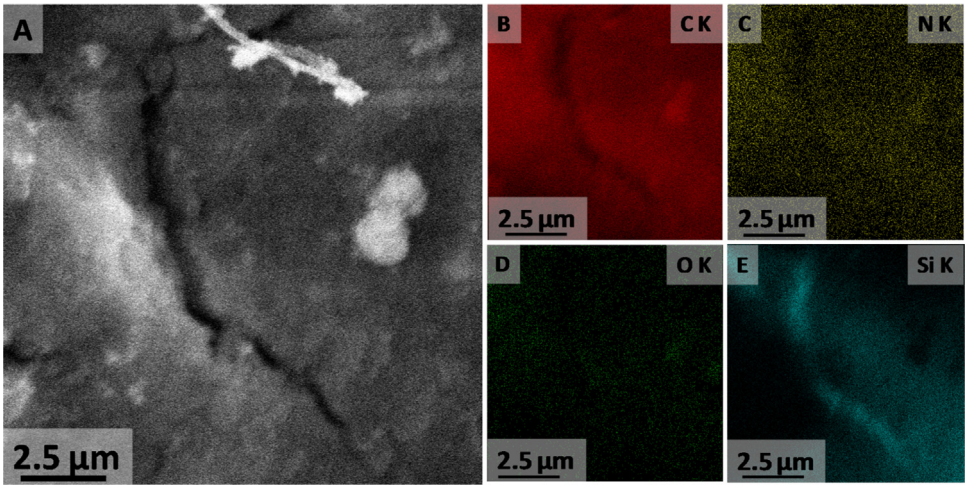

Fig. 3. SEM images of (A) a portion of the ND@NMC phase in the SiC composite and (B-E) the respective EDX elemental mapping. Colors labeling in the elemental maps are: (B) red for C, (C) yellow for N, (D) green for O and (E) light-blue for Si. (For interpretation of the references to colour in this figure legend, the reader is referred to the web version of this article.)

adhesion of the active phase (ND@NMC) at the surface of the macroscopic support (Fig. S3). This test has demonstrated that even after 3 min of sonication in water, the ND@NMC phase remains virtually untouched and the ND@NMC/SiC composite maintains its foamy structure unchanged.

The Brunauer-Emmett-Teller (BET) surface area and pore size distribution for the ND@NMC/SiC sample are shown in Figs. 4 and S4, respectively and compared with those recorded for the pristine SiC foam and the "blank" NMC/SiC composite. Additional chemico-physical details for the above mentioned samples along with those of related literature materials (NDs) and composites (ND/SiC) [50] are outlined in Table 1.

Both NMC/SiC and ND@NMC/SiC samples present type IV isotherms with a distinctive H2 hysteresis loop in the range of 0.4–1.0 P/P_0, typical of mesoporous structures (NMC phase) featured by complex pore networks of ill-defined shape [63]. Finally, the pore-size distribution curves (Fig. S4) show the appearance of mesopore components not present in the pristine SiC foam that largely reflect the increased SSA values measured passing from the pure SiC foam to the NMC/SiC and ND@NMC/SiC composites (28, 57 and 104 m^2/g, respectively). In addition, the ND@MC/SiC without nitrogen doping (14 wt% of ND@MC on the SiC foam) only present the SSA of 96 m^2/g, which could be due to the absence of ammonium carbonate in the precursor solution.

The chemical surface compositions of ND@NMC/SiC and NMC/SiC samples are determined by XPS analyses [31,34,64–66] and they are listed in Table 1 together with that of ND, SiC foam and the literature ND/SiC composite for the sake of comparison. As for the ND@NMC/SiC sample, the XPS survey spectrum (Fig. S5) indicates the presence of C (61.3 at.%), N (10 at.%), O (15.2 at.%) and Si (13.5 at%) with an elemental distribution similar to that measured for the NMC/SiC composite. Both materials present very close N/C ratios, which account for an only minor alteration of the surface composition at the ND@NMC/SiC sample as a consequence of the ND inclusion in the NMC phase. Overall, the moderate growth in the C at% content for the ND@NMC/SiC material, translates in a relatively low ND loading in the catalyst active phase. Finally, the deconvoluted N 1 s core region of ND@NMC/SiC (Fig. 5), presents three main components at 398.5 (52%), 400.2 (27%), and 401.3 eV (16%) attributed to pyridinic, pyrrolic, and quaternary nitrogens, respectively. A minor shoulder (5%) at higher binding energies (403.8 eV) is ascribed to oxidized nitrogen species (Table S1). This N-distribution, confirms the prevalent basic character of the NMC phase, a pre-requisite for a catalyst active phase capable of minimizing the incidence of undesired cracking side-reactions [14,15,34,43–48].

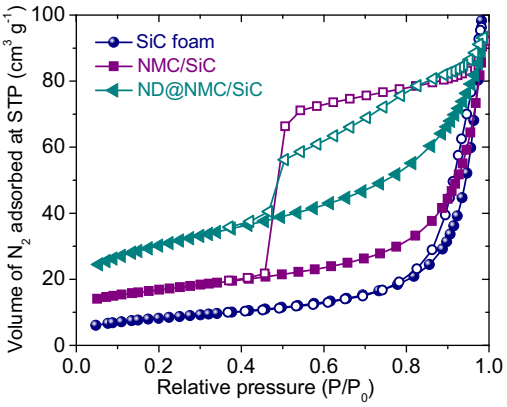

Fig. 4. N_2 adsorption–desorption isotherm linear plots (BET) of SiC (blue curve), NMC/SiC (violet curve) and ND@NMC/SiC (green curve) samples recorded at 77 K. Full dots and empty ones refer to the adsorption and desorption branches, respectively. (For interpretation of the references to colour in this figure legend, the reader is referred to the web version of this article.)

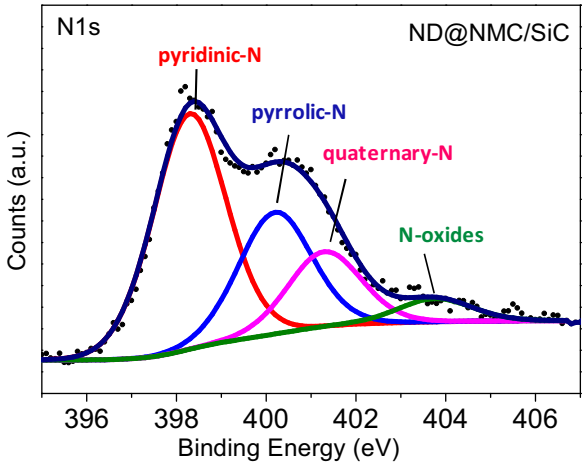

Fig. 5. High-resolution XPS N 1 s core region recorded on the model composite ND@NMC/SiC and its relative peak deconvolution.

3.2. Catalytic performance of ND@NMC/SiC composite

The ND@NMC/SiC composite has successfully been employed as metal-free catalyst for the steam-free, direct (oxygen-free) dehydrogenation of EB at ambient pressure.

Its catalytic performance has been initially scrutinized at 550 °C with 2.8 vol% of EB in He and compared with that of the benchmark Fe-K/Al_2O_3 catalyst (hereafter noted as K-Fe, with 90 wt% of iron loading) under identical conditions. The literature ND/SiC composite and the ND-free NMC/SiC sample have also been evaluated under these operative conditions and their performance are reported in Fig. 6A, B and discussed hereafter for the sake of comparison. For all trials, the amount of catalyst/composite used is fixed to 300 mg in weight. As Fig. 6A shows, all metal-free catalysts exhibit extremely high stability without any significant deactivation at the steady-state conditions (after 20 h on stream) and ST selectivity that remarkably outperform those measured with the K-Fe catalyst. The sharp drop in EB conversion during the first 5 h could be due to the formation of long-chain organic molecules and low graphitized carbons on the surface of the active sites thus covering the surface functional groups, as well as some carbon allotropes rearrangement during the reaction [49]. Thus, it is interesting to investigate the first deactivation period in order to get the insight of the surface reconstruction of catalyst under the reaction conditions in the further work.

In terms of ST rates, all composites present λ values (Fig. 6B) formally ranging from 0.99 (K-Fe) to 1.65 $mmol_{ST}\ g_{cat}^{-1}\ h^{-1}$ (ND@NMC/SiC) that are only apparently lower values than that recorded with pure NDs as catalyst (3.87 $mmol_{ST}\ g_{cat}^{-1}\ h^{-1}$). Indeed, due to the chemical and catalytic inertness of the SiC cores, ST rates for each composite should be properly revised while keeping into account the mass of the relative active phases only (as determined by TGA analyses – ND@NMC for the ND@NMC/SiC, ND for the ND/SiC and NMC for the NMC/SiC). This choice provides a comparison between the different carbon-based materials as much appropriate as possible and offers a valuable cue to debate on the effectiveness of the ND dispersion and loading on the ultimate catalyst performance. On this ground, ST rates have been redrawn accordingly (Fig. 6B, green histograms) thus showing λ values for the two ND-based composites (ND/SiC and ND@NMC/SiC) up to four times higher compared to the bulk NDs. The NMC phase also displays a remarkable ST rate (8.6 $mmol_{ST}g_{cat.act.ph.}^{-1}\ h^{-1}$) that has nearly doubled upon doping with the ND fillers (ND@NMC/SiC: 15.5 $mmol_{ST}g_{cat.act.ph.}^{-1}\ h^{-1}$). For comparison, nitrogen-free ND@MC/SiC composite is also tested

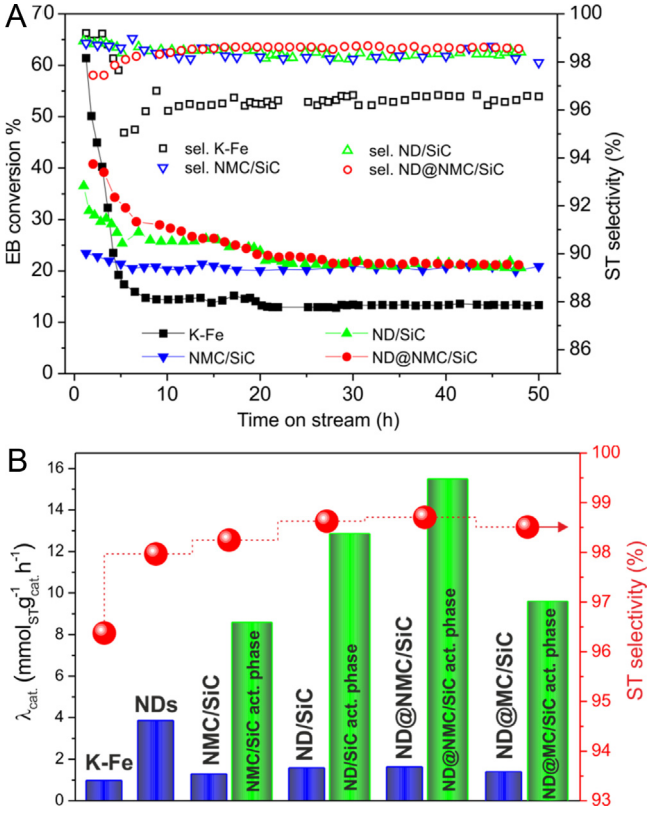

Fig. 6. (A) EB conversions (%) and ST selectivities (%) in the EB DDH promoted by various carbon-based materials and composites. The performance of the benchmarking K-Fe catalyst has been reported under identical experimental conditions for comparison. (B) Specific reaction rates ($\lambda_{cat.}$) (blue bars) and ST selectivity (red spheres) measured with various carbon-based catalysts and the K-Fe system at the steady-state conditions (temperature 550 °C; 2.8 vol.% EB in He at 30 mL min^{-1}). Green bars refer to $\lambda_{act.phase}$ values for all composites as calculated with respect to the effective mass of the active phase only. The reaction results were obtained after 20 h on stream under steady state. (For interpretation of the references to colour in this figure legend, the reader is referred to the web version of this article.)

and gave a ST rate of 9.7 $mmol_{ST}g_{cat.act.ph.}^{-1}\ h^{-1}$, which is much lower than that of ND@NMC/SiC.

The highest λ value measured with ND@NMC/SiC is likely the result of a positive synergistic effect between the ND fillers and the mesoporous NMC phase. This value is even more relevant if we consider the lower ND-loading in the ND@NMC phase respect to that in the ND/SiC composite or compared to that of pure NDs. On this basis, it can be inferred that the homogeneous distribution of the ND fillers in the NMC phase (ND@NMC) maximizes the catalyst performance even in the presence of a very low ND loading.

The ND@NMC/SiC has also been tested in the steam-free EB DDH under (harsh) conditions close to those used in industrial plants (i.e. 600 °C, 10 vol% EB in He) [35,67] where it offers its best performance both in terms of λ value and ST selectivity. Fig. 7A compares ST rates (λ) and selectivity at the steady-state conditions (>20 h on stream) as obtained with both ND-based composites (ND@NMC/SiC and ND/SiC) at 600 °C under different EB concentrations (2.8, 4.7, and 10.0 vol.%). Under these conditions, the ST rate measured for ND/SiC increases steadily passing from 3.7 $mmol_{ST}\ g_{cat}^{-1}\ h^{-1}$ (600 °C, 2.8 vol%) up to 6.4 $mmol_{ST}\ g_{cat}^{-1}\ h^{-1}$ (600 °C, 10 vol%), whereas the ST selectivity drops down to 93% (as average value calculated over the three samples at various EB conc. – see also Table 2). Noteworthy, at increasing EB concentrations (2.8, 4.7 and 10 vol%) the "λ gap" between the two ND-composites (Fig. 7A, blue *vs.* red bars) increases remarkably with the ND@NMC/SiC catalyst ensuring the highest performance both in terms of λ (9.9 $mmol_{ST}\ g_{cat}^{-1}\ h^{-1}$) and

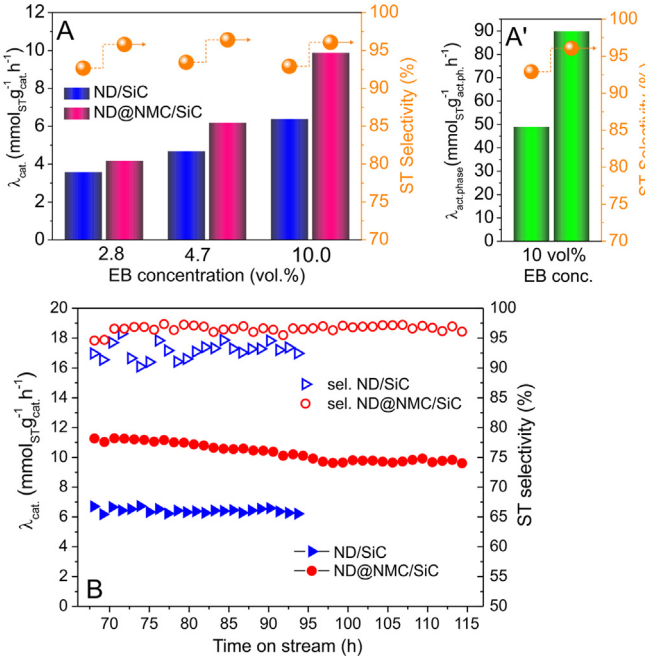

Fig. 7. (A) ST rates and ST selectivity measured for the two ND-based composites at variable EB concentrations and (A') ST rates calculated with respect to the catalysts active phases only. All runs are conducted at 600 °C using from 2.8 to 10 vol.% EB in He, 30 mL min^{-1}. (B) Long-term DDH performance test on ND/SiC and ND@NMC/SiC at 10 vol.% EB concentration (cat. 300 mg, 600 °C, 10 vol% EB in He, 30 mL min^{-1}). The catalytic reaction has also been evaluated in the EB concentration of 2.8 and 4.7 vol%, respectively, at 600 °C over 60 h on-stream (not reported).

Table 2
ND-based composites in the EB DDH as a function of the EB concentration.[a]

Catalyst	EB conc. (vol.%)	X_{EB} (%)	$ST_{sel.}$ (%)	$\lambda_{cat.}$[b]	$\lambda_{act\ phase}$[c]
ND/SiC	2.8[d]	53.0	92.0	3.7	27.5
	4.7	38.1	94.4	4.7	36.4
	10	25.6	93.2	6.4	49.1
ND@NMC/SiC	2.8	56.4	96.0	4.2	37.8
	4.7	49.0	96.4	6.2	56.4
	10	38.3	96.7	9.9	90.0

[a] Reaction conditions: 300 mg of catalyst, 600 °C, 30 mL min^{-1}, atmospheric pressure. The reaction data was obtained after 20 h on stream under steady state.
[b] λ_{cat} is expressed as mmol of ST produced per g of catalyst per hour ($mmol_{ST}\ g_{cat.}^{-1}\ h^{-1}$).
[c] $\lambda_{act\text{-}phase}$ is expressed as mmol of ST produced per g of catalyst active phase per hour ($mmol_{ST} g_{cat.act.ph.}^{-1}\ h^{-1}$).
[d] ND/SiC performance has already been reported elsewhere [50] and quoted here for the sake of comparison.

ST selectivity (up to 96%, as average value over the three samples – see also Table 2). This trend is even more relevant if λ values are re-calculated according to mass of the catalysts active phases only (as determined by TGA analyses – ND@NMC for the ND@NMC/SiC, ND for the ND/SiC). According to that, the ST rate for ND@NMC/SiC is nearly doubled (90.0 $mmol_{ST} g_{cat.act.ph.}^{-1}\ h^{-1}$) with respect to that measured for the ND/SiC composite (49.1 $mmol_{ST} g_{cat.act.ph.}^{-1}\ h^{-1}$) under identical conditions (Fig. 7A' and Table 2).

Moreover, at high EB concentration (10 vol.%) and for long time processes (>100 h), the ND@NMC/SiC sample largely outperforms the catalytic activity and selectivity of the ND/SiC composite. As Fig. 7B shows, the ND@NMC/SiC presents higher ST rate and ST selectivity along with a relatively higher stability on stream compared to its NMC-free counterpart (sel. ND/SiC *vs.* ND@NMC/SiC). These data perfectly match with the higher de-aggregation degree of the ND fillers in the former composite. Indeed, the higher ND dispersion in the NMC phase allows maximizing the contact surface area between the reagent and the catalytically active sites. The NMC phase finally ensures high stability to the composite while its inherent basic character reduces the occurrence of EB side reactions.

We also performed temperature program oxidation coupled with mass spectrometry (TPO-MS) experiments on the ND@NMC/SiC catalyst before and after DDH test at 600 °C and the EB concentration of 10 vol.%. In Fig. S6, it can be found that for the spent catalyst appears an additional CO_2 production peak at the temperature of 670 °C, which could be attributed to the oxidation of the heavy carbonaceous deposition formed during the reaction by polymerisation of the products [67]. This observation would confirm that the deactivation is taking place in the first reaction period of around 30 h, which could be due to the coke deposited on the active phase (Fig. 7B). It is worthy to note that styrene could be the precursor of coke formation at high operation temperature at 600 °C [68]. Interestingly as shown in Fig. 7B, the ND@NMC/SiC presents a markedly higher stability on stream after 30 h on stream. At the end of its life, the regeneration of the exhaust catalyst can be achieved by purging the composite at 450 °C under a diluted oxygen flow (Fig. S7). This simple treatment allows a complete recover of its original performance.

4. Conclusions

In conclusion we have reported the straightforward preparation of a hybrid metal-free catalyst consisting of highly dispersed nanodiamonds within a N-doped mesoporous carbon matrix (NMC) as a tight surface coating for macroscopic β-SiC foam supports. The adopted methodology offers a truly sustainable approach to the generation of a kind of N-doped, carbon porous phase to be used as a non-innocent glue for the homogeneous dispersion of the ND fillers. The as-prepared composite (ND@NMC/SiC) is successfully employed as a highly stable and performing dehydrogenation catalyst for the steam-free and oxygen-free conversion of EB into ST. Both the high ND dispersion within a N-doped mesoporous carbonaceous matrix and the prevalent basic surface character of the NMC phase are two key properties that largely contribute to the improvement of the catalyst performance in the EB DDH. While the first allows to maximize the ND exposure to the reagent throughout the catalytic process, offers a positive synergistic effect to the catalyst ST rate and confers high mechanical resistance to the ND leaching, the second contributes to reduce the incidence of undesired cracking side-reactions.

The best performance of the ND@NMC/SiC composite has been achieved under (severe) conditions close to those used in industrial plants (600 °C and up to 10 vol.% of EB on stream). Under these conditions the catalyst exhibits an extremely high stability for long reactions times with a high coke-resistance and offers superior ST rates and selectivity compared to related composites of the state-of-the-art. Notably, the combination of ND with the mesoporous NMC phase largely preserves the ST selectivity to values close to 97% all over the catalytic process. All these data taken together make the ND@NMC/SiC composite an ideal catalyst candidate suitable for industrial exploitation in the steam-free DDH of EB. It has been calculated that 40 kg of the ND@NMC/SiC composite, containing less than 5.0 kg of the ND@NMC active phase, are sufficient to produce up 1 ton of ST per day under industrial conditions (600 °C and 10 vol.% of EB).

Acknowledgements

Authors thanks the European FP7 project Freecats (contract no. NMP3-SL-2012-280658) and the SATT-Conectus project (DEC-OrATE project no. I14-033) for supporting this research activity. Prof. D. S. Su acknowledges NSFC of China (21473223) for financial

support. Authors also thank Sicat Co. (www.sicatcatalyst.com) for providing SiC supports, T. Romero and S. Sall (ICPEES) for performing SEM and TPO-Mass analyses.

Appendix A. Supplementary data

Supplementary data associated with this article can be found, in the online version, at http://dx.doi.org/10.1016/j.apcatb.2016.07.014.

References

[1] J. Zhang, D.S. Su, R. Blume, R. Schlogl, R. Wang, X.G. Yang, A. Gajovic, Angew. Chem. Int. Ed. 49 (2010) 8640–8644.
[2] F. Cavani, F. Trifiro, Appl. Catal. A: Gen. 133 (1995) 219–239.
[3] O. Shekhah, W. Ranke, R. Schlogl, J. Catal. 225 (2004) 56–68.
[4] M. Muhler, J. Schutze, M. Wesemann, T. Rayment, A. Dent, R. Schlogl, G. Ertl, J. Catal. 126 (1990) 339–360.
[5] M. Muhler, R. Schlogl, G. Ertl, J. Catal. 138 (1992) 413–444.
[6] K.P. Gong, F. Du, Z.H. Xia, M. Durstock, L.M. Dai, Science 323 (2009) 760–764.
[7] D.W. Wang, D.S. Su, Energy Environ. Sci. 7 (2014) 576–591.
[8] G. Tuci, C. Zafferoni, P. D'Ambrosio, S. Caporali, M. Ceppatelli, A. Rossin, T. Tsoufis, M. Innocenti, G. Giambastiani, ACS Catal. 3 (2013) 2108–2111.
[9] K. Chizari, A. Deneuve, O. Ersen, I. Florea, Y. Liu, D. Edouard, I. Janowska, D. Begin, C. Pham-Huu, ChemSusChem 5 (2012) 102–108.
[10] F.G. Sun, J. Liu, H.C. Chen, Z.X. Zhang, W.M. Qiao, D.H. Long, L.C. Ling, ACS Catal. 3 (2013) 862–870.
[11] C. Duong-Viet, H. Ba, Y.F. Liu, L. Truong-Phuoc, J.M. Nhut, C. Pham-Huu, Chin. J. Catal. 35 (2014) 906–913.
[12] Y.F. Liu, C. Duong-Viet, J.J. Luo, A. Hebraud, G. Schlatter, O. Ersen, J.M. Nhut, C. Pham-Huu, ChemCatChem 7 (2015) 2957–2964.
[13] J. Wang, H.Y. Liu, X.M. Gu, H.H. Wang, D.S. Su, Chem. Commun. 50 (2014) 9182–9184.
[14] H. Ba, Y. Liu, L. Truong-Phuoc, C. Duong-Viet, J.-M. Nhut, D.L. Nguyen, O. Ersen, G. Tuci, G. Giambastiani, C. Pham-Huu, ACS Catal. 6 (2016) 1408–1419.
[15] Z. Zhao, Y. Dai, G. Ge, Catal. Sci. Technol. 5 (2015) 1548–1557.
[16] V.N. Mochalin, O. Shenderova, D. Ho, Y. Gogotsi, Nat. Nanotech. 7 (2012) 11–23.
[17] A. Krueger, Adv. Mater. 20 (2008) 2445–2449.
[18] S. Sotoma, K. Akagi, S. Hosokawa, R. Igarashi, H. Tochio, Y. Harada, M. Shirakawa, RSC Adv. 5 (2015) 13818–13827.
[19] J. Wehling, R. Dringen, R.N. Zare, M. Maas, K. Rezwan, ACS Nano 8 (2014) 6475–6483.
[20] T. Zhang, A. Neumann, J. Lindlau, Y.Z. Wu, G. Prarnanik, B. Naydenov, F. Jelezko, F. Schuder, S. Huber, M. Huber, F. Stehr, A. Hogele, T. Weil, T. Liedl, J. Am. Chem. Soc. 137 (2015) 9776–9779.
[21] F. Zhang, Q.X. Song, X. Huang, F.N. Li, K. Wang, Y.X. Tang, C.L. Hou, H.X. Shen, ACS Appl. Mater. Inter 8 (2016) 1087–1097.
[22] Z.Q. Xue, J.C. Vinci, L.K. Colon, ACS Appl. Mater. Interfaces 8 (2016) 4149–4157.
[23] B.T. Miles, A.B. Greenwood, B.R. Patton, H. Gersen, ACS Photonics 3 (2016) 343–348.
[24] M. Alishiri, A. Shojaei, M.J. Abdekhodaie, RSC Adv. 6 (2016) 8743–8755.
[25] Z.K. Zhao, W.Z. Li, Y.T. Dai, G.F. Ge, X.W. Guo, G.R. Wang, ACS Sus. Chem. Eng. 3 (2015) 3355–3364.
[26] N. Gupta, Y.X. Ding, Z.B. Feng, D.S. Su, ChemCatChem 8 (2016) 922–928.
[27] Z.K. Zhao, Y.T. Dai, G.F. Ge, G.R. Wang, ChemCatChem 7 (2015) 1135–1144.
[28] X. Duan, C. Su, L. Zhou, H. Sun, A. Suvorova, T. Odedairo, Z. Zhu, Z. Shao, S. Wang, Appl. Catal. B: Environ. 194 (2016) 7–15.
[29] S. Osswald, G. Yushin, V. Mochalin, S.O. Kucheyev, Y. Gogotsi, J. Am. Chem. Soc. 128 (2006) 11635–11642.
[30] O. Shenderova, A. Koscheev, N. Zaripov, I. Petrov, Y. Skryabin, P. Detkov, S. Turner, G. Van Tendeloo, J. Phys. Chem. C 115 (2011) 9827–9837.
[31] Y.M. Lin, D.S. Su, ACS Nano 8 (2014) 7823–7833.
[32] T.T. Thanh, H. Ba, T.P. Lai, J.M. Nhut, O. Ersen, D. Begin, I. Janowska, D.L. Nguyen, P. Granger, C. Pham-Huu, J. Mater. Chem. A 2 (2014) 11349–11357.
[33] H. Liu, J. Diao, Q. Wang, S. Gu, T. Chen, C. Miao, W. Yang, D. Su, Chem. Commun. 50 (2014) 7810–7812.
[34] Z.K. Zhao, Y.T. Dai, J. Mater. Chem. A 2 (2014) 13442–13451.
[35] H. Ba, L. Truong-Phuoc, Y. Liu, C. Duong-Viet, J.-M. Nhut, L. Nguyen-Dinh, P. Granger, C. Pham-Huu, Carbon 96 (2016) 1060–1069.
[36] D. Guo, R. Shibuya, C. Akiba, S. Saji, T. Kondo, J. Nakamura, Science 351 (2016) 361–365.
[37] G. Tuci, C. Zafferoni, A. Rossin, L. Luconi, A. Milella, M. Ceppatelli, M. Innocenti, Y.F. Liu, C. Pham-Huu, G. Giambastiani, Catal. Sci. Tench. (2016), http://dx.doi.org/10.1039/c6cy00796a.
[38] Z.K. Zhao, Y.T. Dai, G.F. Ge, X.W. Guo, G.R. Wang, Phys. Chem. Chem. Phys. 17 (2015) 18895–18899.
[39] Z.K. Zhao, Y.T. Dai, G.F. Ge, X.W. Guo, G.R. Wang, RSC Adv. 5 (2015) 53095–53099.
[40] Z.K. Zhao, Y.T. Dai, G.F. Ge, G.R. Wang, AIChE J. 61 (2015) 2543–2561.
[41] Z.K. Zhao, Y.T. Dai, G.F. Ge, G.R. Wang, Chem. Eur. J. 21 (2015) 8004–8009.
[42] J. Wang, H.Y. Liu, J.Y. Diao, X.M. Gu, H.H. Wang, J.F. Rong, B.N. Zong, D.S. Su, J. Mater. Chem. A 3 (2015) 2305–2313.
[43] Z. Zhao, Y. Dai, J. Lin, G. Wang, Chem. Mater. 26 (2014) 3151–3161.
[44] Z. Zhao, Y. Dai, G. Ge, X. Guo, G. Wang, Green Chem. 17 (2015) 3723–3727.
[45] Z. Zhao, T. Dai, G. Ge, Q. Mao, Z. Rong, G. Wang, ChemCatChem 7 (2015) 1070–1077.
[46] Y.V. Kissin, Catal. Rev.: Sci. Eng. 43 (2001) 85–146.
[47] X. Jin, V.V. Balasubramanian, S.T. Selvan, D.P. Sawant, M.A. Chari, G.Q. Lu, A. Vinu, Angew. Chem. Int. Ed. 48 (2009) 7884–7887.
[48] R. Gounder, E. Iglesia, J. Am. Chem. Soc. 131 (2009) 1958–1971.
[49] H. Ba, S. Podila, Y.F. Liu, X.K. Mu, J.M. Nhut, V. Papaefthimiou, S. Zafeiratos, P. Granger, C. Pham-Huu, Catal. Today 249 (2015) 167–175.
[50] H. Ba, Y.F. Liu, X.K. Mu, W.H. Doh, J.M. Nhut, P. Granger, C. Pham-Huu, Appl. Catal. A: Gen. 499 (2015) 217–226.
[51] H. Ba, Y. Liu, L. Truong-Phuoc, C. Duong-Viet, X. Mu, W.H. Doh, T. Tran-Thanh, W. Baaziz, L. Nguyen-Dinh, J.-M. Nhut, I. Janowska, D. Begin, S. Zafeiratos, P. Granger, G. Tuci, G. Giambastiani, F. Banhart, M.J. Ledoux, C. Pham-Huu, Chem. Commun. 51 (2015) 14393–14396.
[52] L. Borchardt, C. Hoffmann, M. Oschatz, L. Mammitzsch, U. Petasch, M. Herrmann, S. Kaskel, Chem. Soc. Rev. 41 (2012) 5053–5067.
[53] Y. Liu, O. Ersen, C. Meny, F. Luck, C. Pham-Huu, ChemSusChem 7 (2014) 1218–1239.
[54] X.Y. Li, X.L. Pan, L. Yu, P.J. Ren, X. Wu, L.T. Sun, F. Jiao, X.H. Bao, Nat. Commun. 5 (2014) http://dx.doi.org/10.1038/ncomms4688.
[55] Y.F. Liu, B. de Tymowski, F. Vigneron, I. Florea, O. Ersen, C. Meny, P. Nguyen, C. Pham, F. Luck, C. Pham-Huu, ACS Catal. 3 (2013) 393–404.
[56] R. Dhiman, E. Johnson, E.M. Skou, P. Morgen, S.M. Andersen, J. Mater. Chem. A 1 (2013) 6030–6036.
[57] J.Y. Hao, Y.Y. Wang, X.L. Tong, G.Q. Jin, X.Y. Guo, Int. J. Hydrogen Energy 37 (2012) 15038–15044.
[58] S. Hajiesmaili, S. Josset, D. Begin, C. Pham-Huu, N. Keller, V. Keller, Appl. Catal. A Gen. 382 (2010) 122–130.
[59] A.N. Kouame, R. Masson, D. Robert, N. Keller, V. Keller, Catal. Today 209 (2013) 13–20.
[60] Y. Liu, I. Florea, O. Ersen, C. Pham-Huu, C. Meny, Chem. Commun. 51 (2015) 145–148.
[61] M. Lacroix, L. Dreibine, B. de Tymowski, F. Vigneron, D. Edouard, D. Bégin, P. Nguyen, C. Pham, S. Savin-Poncet, F. Luck, M.-J. Ledoux, C. Pham-Huu, Appl. Catal. A Gen. 397 (2011) 62–72.
[62] L. Truong-Phuoc, T.H. Tri, N.D. Lam, W. Baaziz, T. Romero, D. Edouard, D. Begin, I. Janowska, C. Pham-Huu, Appl. Catal. A Gen. 469 (2014) 81–88.
[63] K.S.W. Sing, D.H. Everett, R.A.W. Haul, L. Moscou, R.A. Pierotti, J. Rouquérol, Pure Appl. Chem. 57 (1985) 603–619.
[64] X.G. Duan, H.Q. Sun, Y.X. Wang, J. Kang, S.B. Wang, ACS Catal. 5 (2015) 553–559.
[65] Y.M. Lin, X.L. Pan, W. Qi, B.S. Zhang, D.S. Su, J. Mater. Chem. A 2 (2014) 12475–12483.
[66] Z.H. Sheng, L. Shao, J.J. Chen, W.J. Bao, F.B. Wang, X.H. Xia, ACS Nano 5 (2011) 4350–4358.
[67] I. Rossetti, E. Bencini, L. Trentini, L. Forni, Appl. Catal. A: Gen. 292 (2005) 118–123.
[68] M. Baghalha, O. Ebrahimpour, Appl. Catal. A: Gen. 326 (2007) 143–151.